Ivo DOLEŽEL[1], Václav KOTLAN[2], Bohuš ULRYCH[2]

[1]Academy of Sciences of the Czech Republic in Prague, Czech Republic, [2]University of West Bohemia in Pilsen, Czech Republic

Electromagnetic-thermoelastic actuator for accurate wide-range setting of position

Abstract. *A novel actuator for accurate setting of position is presented, allowing a wide-range shift. While the rougher setting of position is realized electromagnetically, its fine tuning is performed on the principle of thermoelastic dilatation of the nonferromagnetic part of the plunger. The complete mathematical model of the problem (representing a triply coupled task) is solved numerically. The methodology is illustrated by an example whose results are discussed.*

Streszczenie. *W artykule przedstawiono nowy projekt aktuatora o szerokim zakresie przemieszczeń. Zgrubne pozycjonowanie jest realizowane za pomocą sterowania elektromagnetycznego, natomiast precyzyjne dostrojenie pozycji osiąga się przez termoelastyczną dylatację nie-ferromagnetycznego elementu trzpienia. Rozwiązano numerycznie kompletny matematyczny model urządzenia (uwzględniający sprzężenia pól). Zaprezentowana metody została zilustrowana przykładowymi obliczeniami, których wyniki zostały starannie przeanalizowane. (**Siłownik termoelastyczny o szerokim zakresie przemieszczeń**)*

Keywords: actuator, electromagnetic field, temperature field, field of thermoelastic displacements, setting of position, numerical analysis.
Slowa kluczowe: siłownik, pole elektromagnetyczne, odkształcenie termoelastyczne.

Introduction

Setting of position in technical practice may be realized by a number of ways derived from numerous mechanical, hydraulic, pneumatic, electromagnetic and other principles. The main disadvantage of these systems consists in the presence of movable parts (screws, pistons, plungers, etc.) whose movement negatively affects the available accuracy of such devices.

In their previous papers (see, for example [1], [2]) the authors proposed a purely thermoelastic actuator that worked sufficiently accurately without any movable parts, but only with extremely small shifts (10^{-5}–10^{-3} m). Possibilities of applications of such actuators, therefore, suffered from rather high setting limitations.

The paper presents a novel actuator combining a classical electromagnetic device of this kind with thermoelasticity. The device allows accurate setting of position in a wide range of distances.

Description of the device

The schematic arrangement of the device is depicted in Fig. 1. Its working regime consists of two steps.

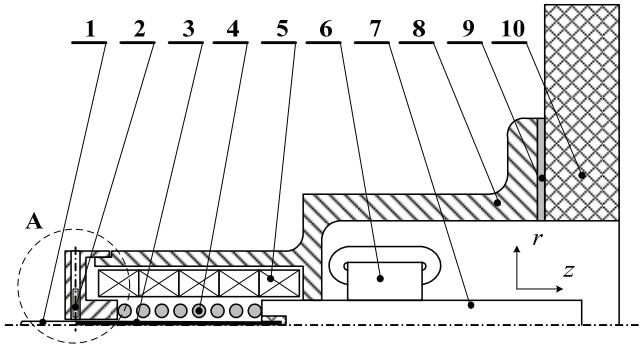

Fig. 1. A combined electromagnetic-thermoelastic actuator: **1**–ceramic part of the plunger, **2**–electromagnetic clutch I, **3**–nonferromagnetic metal part of the plunger, **4**–return spring, **5**–field coil consisting of several sections, **6**–electromagnetic clutch II, **7**–ferromagnetic part of the plunger, **8**–ferromagnetic shell of the device, **9**–thermal insulation, **10**–stiff frame or wall

A. Electromagnetic regime (rough setting)

The field coil **5** is connected to the source of direct current (DC). Its magnetic field produces force acting on the ferromagnetic part **7** of the plunger, pulling it into the coil. This force must be higher than the counterforce produced by the return spring **4** (and possible external force). After reaching the desired shift ς (fast, but only approximate), the friction clutch **6** switches on while the field coil **5** is disconnected from the DC source. Now the position of the plunger is fixed, but still it may exhibit a certain error.

B. Thermoelastic regime

Selected sections of the coil **5** are connected to a source of harmonic current that generates periodical magnetic field in the device. This field induces in the plunger (mainly in its nonferromagnetic part **3**) eddy currents producing there the Joule losses that cause its heating and consequent dilatation u_z with respect to its fixed part – friction surface of the friction clutch **6**. After reaching the desired accurate position the field coil **5** is disconnected from the source and electromagnetic clutch **2** fixes the position of the leftmost ceramic part **1** of the plunger (whose thermal dilatability is negligible). At the same time, the friction clutch **6** is disconnected, so that the right (ferromagnetic) part of the plunger will completely get free.

Mathematical model and its solution

The arrangement of the device may be considered axisymmetric. Its complete model consists of several partial models providing the results for both above regimes:

- for the electromagnetic regime we need to know the static characteristics of the device together with the operation of the friction clutch **6** (friction force and temperature rise),
- for the thermoelastic regime we determine the distribution of periodical magnetic field in the system, temperature rise of the plunger (particularly its nonferromagnetic part) and its dilatation.

A. Electromagnetic regime

A.1 Electromagnetic part of the actuator

The principal quantity to find is its static characteristic (i.e., the dependence of the electromagnetic force F_{m} on the shift ς of the plunger, see Fig. 2). Its knowledge is of extreme importance for finding the position at which the electromagnetic regime should stop.

If we neglect the time evolution of direct current in the field coil, the static characteristic can be determined as follows:

- For a sufficient number of shifts of the plunger we calculate the distribution of magnetic field (described in terms of magnetic vector potential $\boldsymbol{A}$) in the device using the equation [3]

(1) $$\operatorname{curl}\left(\frac{1}{\mu}\operatorname{curl}\boldsymbol{A}\right)=\boldsymbol{J}_{\mathrm{ext,DC}}$$

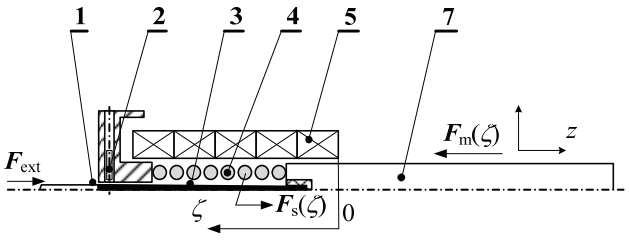

Fig. 2. To the computation of the static characteristic $\boldsymbol{F}_{\mathrm{m}}=\boldsymbol{F}_{\mathrm{m}}(\zeta)$ of the device (the positions correspond to Fig. 1)

where μ is the magnetic permeability and $\boldsymbol{J}_{\mathrm{ext,DC}}$ is the field current density.

- The magnetic force $\boldsymbol{F}_{\mathrm{m}}$ acting on the ferromagnetic movable part **7** of the plunger is expressed by the integral

(2) $$\boldsymbol{F}_{\mathrm{m}}=\frac{1}{2}\oint_{S_7}\left[\boldsymbol{H}(\boldsymbol{n}\cdot\boldsymbol{B})+\boldsymbol{B}(\boldsymbol{n}\cdot\boldsymbol{H})-\boldsymbol{n}(\boldsymbol{H}\cdot\boldsymbol{B})\right]\mathrm{d}S\,,$$

where $\boldsymbol{H}$ and $\boldsymbol{B}$ are vectors of the magnetic field, $\boldsymbol{n}$ denotes the unit vector of the outward normal, and finally, S_7 is the surface of the movable part **7**. The force $\boldsymbol{F}_{\mathrm{m}}$ (that depends on the instantaneous position ζ of the plunger) must be always higher than the counterforce $\boldsymbol{F}_{\mathrm{s}}$ produced by the return spring **4** (which is also a function of position ζ) and possible external force $\boldsymbol{F}_{\mathrm{ext}}$ (see Fig. 2). This condition may be expressed by the inequality

(3) $$\left|\boldsymbol{F}_{\mathrm{m}}(\zeta)\right|\geq\left|\boldsymbol{F}_{\mathrm{s}}(\zeta)+\boldsymbol{F}_{\mathrm{ext}}\right|$$

The above mechanical transient is very short (on the order of 10^{-2}–10^{-1} s). The temperature rise of the system due to the Joule losses in the field coil is, therefore, very low and in practical computations it can be neglected without any significant error.

A.2 Electromagnetic clutch ***6***

As soon as the plunger roughly reaches the desired position, the field coil **5** is disconnected from the source of direct current, while the magnetic friction clutch **6** (whose arrangement is schematically depicted in Fig. 3) controlled by direct current switches on. Let the value of this current be $I_{\mathrm{ext,C}}$ and its density $\boldsymbol{J}_{\mathrm{ext,C}}$. The magnetic force $\boldsymbol{F}_{\mathrm{mC}}$ produced by the clutch is also calculated from the model given by (1) and (2) (but now, the integration in (2) must be carried out over the whole surface of the clutch).

The normal component $F_{\mathrm{mC,n}}$ of the force $\boldsymbol{F}_{\mathrm{mC}}$ with respect to its jaws then produces the axial friction force $\boldsymbol{F}_{\mathrm{f}}$ between the jaws of the clutch and the plunger to be fixed. Its value is

(4) $$\left|\boldsymbol{F}_{\mathrm{f}}\right|=F_{\mathrm{f,a}}=f\,F_{\mathrm{mC,n}}\,,$$

where f denotes the friction coefficient and $F_{\mathrm{f,a}}$ is the axial component of the friction force. Again it must hold that

(5) $$\left|\boldsymbol{F}_{\mathrm{f}}\right|\geq\left|\boldsymbol{F}_{\mathrm{s}}(\zeta)+\boldsymbol{F}_{\mathrm{ext}}\right|.$$

During its operation that may take a long time (minutes), the field coil **4** heats up. Its temperature rise causes corresponding temperature rise of other parts of the system, mainly due to convection (the coil itself is insulated). As for the parasitic temperature rise of the plunger, it should be as low as possible in order not to influence its behavior in the following thermoelastic regime.

The nonstationary temperature field in the clutch is described by the equation [4]

(6) $$\operatorname{div}(\lambda\operatorname{grad}T)=\rho c\frac{\partial T}{\partial t}-p_{\mathrm{J}}\,,$$

where λ stands for the thermal conductivity, ρ is the specific mass, c denotes the specific heat, and symbol p_{J} denotes the volumetric ohmic losses produced in the field coil 4 (see Fig. 3). Their value is

(7) $$p_{\mathrm{J}}=\frac{\boldsymbol{J}_{\mathrm{ext,C}}^2}{\gamma}\,,$$

where γ is the electrical conductivity of material of the field coil. Both quantities in (7) should be recalculated with respect to the corresponding coefficient of filling.

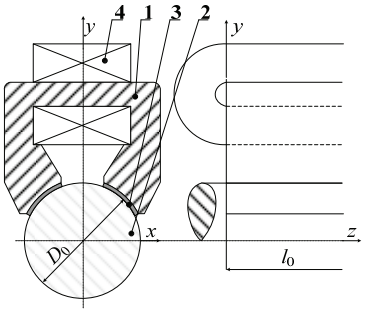

Fig. 3. Basic arrangement of the considered friction clutch: **1**–ferromagnetic frame of the clutch, **2**–ferromagnetic part of the plunger whose position is to be fixed, **3**–friction relining of the jaws of the clutch, **4**–field coil

B. Thermoelastic regime

B.1 Thermoelastic part of the actuator

The thermoelastic regime is characterized by induction heating of the nonferromagnetic part **3** of the plunger and its consequent dilatation. The model of this process represents a task coupling the electromagnetic field, temperature field and field of thermoelastic displacements.

Distribution of the *periodical electromagnetic* field in the system is now given by the solution of the well-known parabolic equation for magnetic vector potential $\boldsymbol{A}$ in the form

(8) $$\operatorname{curl}\left(\frac{1}{\mu}\operatorname{curl}\boldsymbol{A}\right)+\gamma\frac{\partial\boldsymbol{A}}{\partial t}=\boldsymbol{J}_{\mathrm{ext,AC}}\,,$$

where γ is the electric conductivity and $\boldsymbol{J}_{\mathrm{ext,AC}}$ denotes the vector of the external harmonic current density in the field coil. But solution to (8) would require a lot of time because the steady state is reached only after several (about 10) periods of the field current (which could represents at least 10^3 time steps) and, on the other hand the influence of that short transient on the temperature field can be expected practically negligible. That is why we decided to simplify the model using the assumption that the magnetic field is harmonic. In such a case it can be described by the Helmholtz equation for the phasor $\underline{\boldsymbol{A}}$ of the magnetic vector potential $\boldsymbol{A}$

(9) $$\operatorname{curlcurl}\underline{\boldsymbol{A}}+\mathrm{j}\cdot\omega\gamma\mu\underline{\boldsymbol{A}}=\mu\underline{\boldsymbol{J}}_{\mathrm{ext,AC}}\,,$$

where ω is the angular frequency. But the magnetic permeability μ of ferromagnetic parts is not supposed

constant; it is always assigned to the local value of magnetic flux density $\boldsymbol{B}$ (that is, of course, also harmonic similarly as the field of $\boldsymbol{A}$). Its computation is based on an iterative procedure (that is, moreover, implemented in some professional electromagnetic codes).

The nonstationary *temperature field* in the system is described by the heat transfer equation (6). Here the symbol p denotes the time average internal volume sources of heat that generally consist of the volumetric Joule losses p_{J} due to eddy currents and volumetric magnetization losses p_{m}

$$p = p_{\mathrm{J}} + p_{\mathrm{m}}, \tag{10}$$

where

$$p_{\mathrm{J}} = \left|\underline{\boldsymbol{J}}_{\mathrm{eddy}}\right|^2 / \gamma, \quad \underline{\boldsymbol{J}}_{\mathrm{eddy}} = \mathrm{j}\cdot\omega\gamma\underline{\boldsymbol{A}}, \tag{11}$$

while p_{m} must be determined from the known measured loss dependence $p_{\mathrm{m}} = p_{\mathrm{m}}\left(\left|\underline{\boldsymbol{B}}\right|\right)$ for the used ferromagnetic material.

The solution of the *thermoelastic problem* may be performed in several manners. After some research in the domain we decided to use the Lamé equation for the vector of displacements $\boldsymbol{u}$ that reads [5]

$$\begin{aligned}&\left(\varphi+\psi\right)\cdot\mathrm{grad}\left(\mathrm{div}\,\boldsymbol{u}\right)+\psi\cdot\Delta\boldsymbol{u}-\\&-\left(3\varphi+2\psi\right)\cdot\alpha_{\mathrm{T}}\cdot\mathrm{grad}\,T+\boldsymbol{f}=\boldsymbol{0},\end{aligned} \tag{12}$$

where $\varphi \geq 0, \psi > 0$ are the Lamé coefficients associated with material parameters by the relations

$$\varphi = \frac{\nu\cdot E}{\left(1+\nu\right)\left(1-2\nu\right)}, \quad \psi = \frac{E}{2\left(1+\nu\right)}. \tag{13}$$

Here E denotes the modulus of elasticity and ν the Poisson coefficient of the transverse contraction. Finally, $\boldsymbol{u} = \left(u_r, u_\varphi, u_z\right)$ represents the displacement vector, α_{T} the coefficient of the linear thermal dilatability of material and $\boldsymbol{f}$ the vector of the internal volumetric forces.

B.2 Electromagnetic clutch ***2***

The clutch is used for fixing the dilatation element at the moment when it reaches the desired position. At the same time the clutch **6** is disconnected from the source of the field current in order that it right end (see Fig. 1) would get free.

The schematic arrangement of this clutch (detail **A** in Fig. 1) is depicted in Fig. 4.

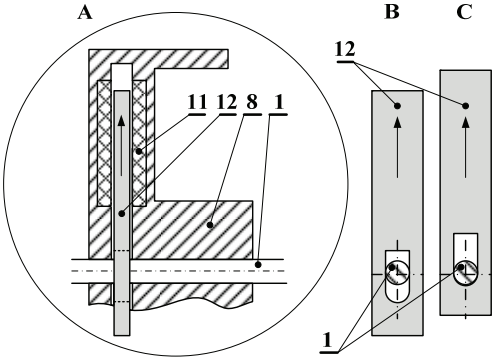

Fig. 4. Schematic arrangement of magnetic clutch **2**: **1**–ceramic part of the plunger of the thermoelastic actuator, **8**–ferromagnetic shell, **11**–field coil, **12**–plunger

Symbols **B** and **C** in Fig. 4 denote the starting and final position of the plunger **12**, respectively. When the ceramic part **1** of the main plunger shifts (due to thermoelastic dilatations), the field coil **11** of the clutch is off. When it reaches the desired position, the coil **11** is connected to the source of current and pulls the plunger **12** in. The plunger starts exerting a normal force to ceramic part **1** and the consequent friction forces stop its further movement. At the same moment the magnetic clutch **6** is disconnected.

The force effects are determined using the model described by (1) and (2)

Numerical solution and computer model

The mathematical model presented in the previous paragraph was solved by the finite element method (FEM) using the codes QuickField [6] and COMSOL Multiphysics [7] supplemented with a lot of own procedures and scripts. Particular attention was paid to the convergence of results (in the case of the thermoelastic regime) in the dependence of the position of the artificial boundary and density of the discretization mesh. In order to obtain values with three valid digits for the magnetic field, the mesh for magnetic field had to consist of more than 150 000 elements; for the two remaining fields this number could be substantially lower (the corresponding definition areas are smaller and both fields are relatively smooth) – about 50000 and 30000 elements.

Illustrative example

We modeled several arrangements differing by both dimensions and used materials. All of them were more or less similar to that in Fig. 1. For an illustration, we will present the most important results for the device whose principal dimensions are depicted in Fig. 5. This device does not contain the magnetic clutch **2** (but its presence influences the main results by not more than about 2–3 %) and ceramic part of the plunger.

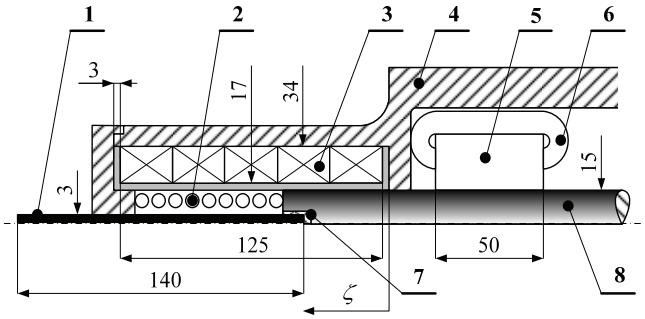

Fig. 5. The main part of the investigated device with the principal dimensions in mm: **1**–nonferromagnetic part of the plunger, **2**–return spring, **3**–field coil of the actuator, **4**–ferromagnetic shell, **5**–magnetic circuit of the friction clutch, **6**–field coil of the clutch, **7**–connecting Teflon matrix, **8**–ferromagnetic part of the plunger

The main physical properties of the parts depicted in Fig. 1 are listed in Table 1.

Table 1. Physical properties of parts depicted in Fig. 5

No.	Material	Parameter	Value	Dimension
1	Zn	relative magnetic permeability μ_{r}	1	(-)
		thermal conductivity λ	116	(W/m K)
		electrical conductivity γ	1.666×10^{7}	(S/m)
		Young modulus E	1.0×10^{11}	(N/m^2)

		Poisson number ν	0.25	(-)
		coef. thermal dilatability α_T	2.9×10^{-5}	(1/K)
2	spring steel DIN 17 221	relative magnetic permeability μ_r	1	(-)
		shear module G	7.8×10^{4}	(N/m^2)
		maximum temperature T_{work}	200	(°C)
3	Cu	diameter of the conductor D_c	1	(mm)
		number of turns N_3	1250	(-)
		coefficient of filling κ	0.785	(-)
		relative magnetic permeability μ_r	1	(-)
		thermal conductivity λ *	306.1	(W/m K)
		electrical conductivity γ *	4.474×10^{7}	(S/m)
4 **5** **8**	carbon steel 12 040	magnetization characteristic $B(H)$ see Fig. 6		
		thermal conductivity $\lambda(T)$ see Fig. 7	306.1	(W/m K)
		electrical conductivity γ	6.666×10^{6}	(S/m)
		Young modulus E	2.1×10^{11}	(N/m^2)
		Poisson number ν	0.3	(-)
		coef. thermal dilatability α_T	1.25×10^{-5}	(1/K)
6	Cu	diameter of the conductor D_c	1	(mm)
		number of turns N_6	1250	(-)
		other parameters see No. **3**		
7	Teflon	relative magnetic permeability μ_r	1	(-)
		thermal conductivity λ	1.6	(W/m K)

* Electrical conductivity of material of both coils **3** and **6** is recalculated with respect to their coefficients of filling.

The air inside the device is supposed unmoving, its thermal conductivity being 0.03 W/mK.

The computations provided a lot of results. The most important ones are depicted in several following figures. Figure 8 shows the distribution of stationary magnetic field in the device in the electromagnetic regime, for $\varsigma = 50$ mm and $J_{ext,DC} = 5\times10^{6}$ A/m^2. It is obvious that magnetic field does not penetrate to more distant parts of the ferromagnetic shell (the rightmost parts of the device, therefore, are not depicted).

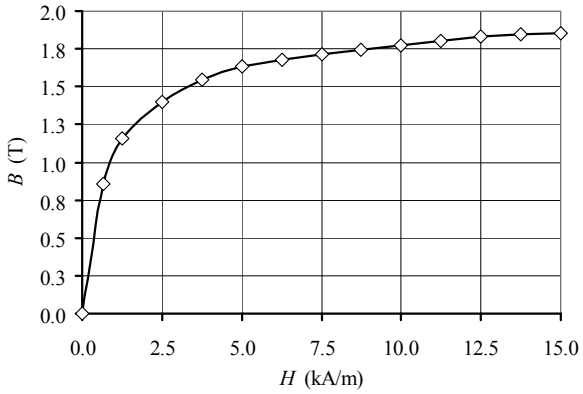

Fig. 6. Magnetization characteristic of carbon steel 12 040

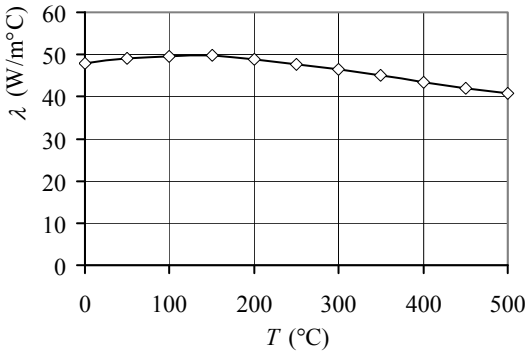

Fig. 7. Temperature dependence of thermal conductivity λ of carbon steel 12 040

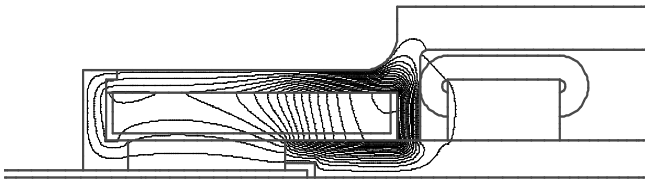

Fig. 8. Distribution of stationary magnetic field in the system for $\varsigma = 50$ mm and $J_{ext,DC} = 5\times10^{6}$ A/m^2

Figure 9 shows another field distribution when the field coil carries harmonic current (thermoelastic regime) for $\varsigma = 25$ mm, $J_{ext,AC} = 5\times10^{6}$ A/m^2 and $f = 5$ kHz.

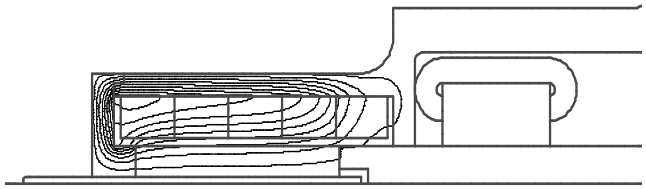

Fig. 9. Distribution of harmonic magnetic field in the system for $\varsigma = 25$ mm, $J_{ext,AC} = 5\times10^{6}$ A/m^2, and $f = 5$ kHz

Figure 10 depicts the steady-state distribution of temperature in the device for $\varsigma = 25$ mm,

$J_{\mathrm{ext,AC}} = 10^6$ A/m^2, and $f = 5$ kHz. The maximum gradient of temperature is, of course, in the nonferromagnetic (zinc) part of the plunger. The maximum temperature in the system $T_{\max} = 54$ °C, the difference between two neighboring isotherms being $\Delta T = 3$ °C.

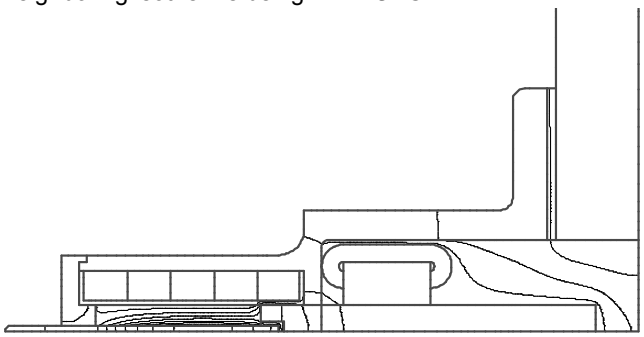

Fig. 10. Distribution of steady-state temperature field in the system for $\varsigma = 25$ mm, $J_{\mathrm{ext,AC}} = 10^6$ A/m^2, $f = 5$ kHz, $T_{\max} = 54$ °C, and $\Delta T = 3$ °C

Figure 11 shows the final thermoelastic displacements of the nonferromagnetic part of the plunger (exaggerated for better visibility) on the following conditions: $\varsigma = 25$ mm, $J_{\mathrm{ext,AC}} = 10^6$ A/m^2, and $f = 5$ kHz.

Fig. 11. Distribution of steady-state thermoelastic displacements of the zinc part of the plunger for $\varsigma = 25$ mm, $J_{\mathrm{ext,AC}} = 10^6$ A/m^2, $f = 5$ kHz

The previous figures are, however, rather illustrative, in order to obtain a good idea about the distribution of particular physical fields. More important (in our opinion) is the following series of figures that summarize the results obtained.

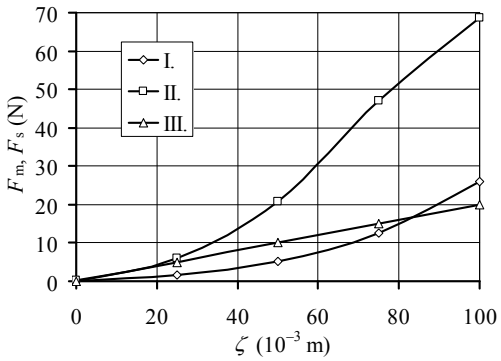

Fig. 12. Dependencies of the magnetic force F_{m} and counterforce F_{s} exerted by the return spring on shift ς; I - $F_{\mathrm{m}}(\varsigma)$ for DC field current density $J_{\mathrm{ext,DC}} = 10^6$ A/m^2, II - $F_{\mathrm{m}}(\varsigma)$ for DC field current density $J_{\mathrm{ext,DC}} = 2 \times 10^6$ A/m^2, III - $F_{\mathrm{s}}(\varsigma)$ for the constant of elasticity $k = 0.2$ N/m

Figure 12 shows the dependencies of the magnetic force F_{m} on shift ς for two different values of DC field current density $J_{\mathrm{ext,DC}}$ and a similar dependence of the counterforce $F_{\mathrm{s}}(\varsigma)$ exerted by the return spring. It is clear that for the selected return spring the current density $J_{\mathrm{ext,DC}} = 10^6$ A/m^2 is to low to overcome the counterforce $F_{\mathrm{s}}(\varsigma)$ (the plunger would not move at all). But DC field current density $J_{\mathrm{ext,DC}} = 2 \times 10^6$ A/m^2 is already enough for the movement of the plunger in any range of shifts ($F_{\mathrm{m}} > F_{\mathrm{s}}$ everywhere).

The same conclusion can be seen in Fig. 13 that depicts the resultant static characteristics of the electromagnetic regime (defined as $F_{\mathrm{tot}} = F_{\mathrm{m}} - F_{\mathrm{s}}$) for three different DC field current densities and the same elasticity constant of the return spring.

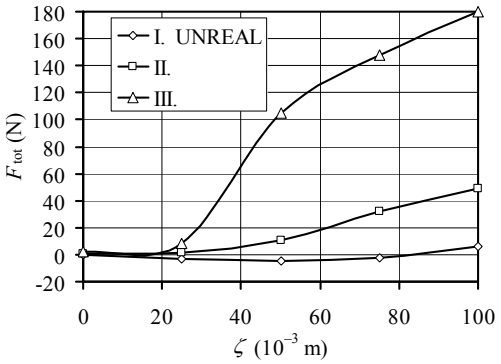

Fig. 13. Static characteristics of the device for I - $J_{\mathrm{ext,DC}} = 10^6$ A/m^2, II - $J_{\mathrm{ext,DC}} = 2 \times 10^6$ A/m^2, III - $J_{\mathrm{ext,DC}} = 5 \times 10^6$ A/m^2

Figure 14 shows the dependence of the total thermoelastic shift u_z of the leftmost point of the zinc part of the plunger on its average temperature T_{av} when the previous electromagnetic shift $\varsigma = 25$ mm. The dependence is almost linear.

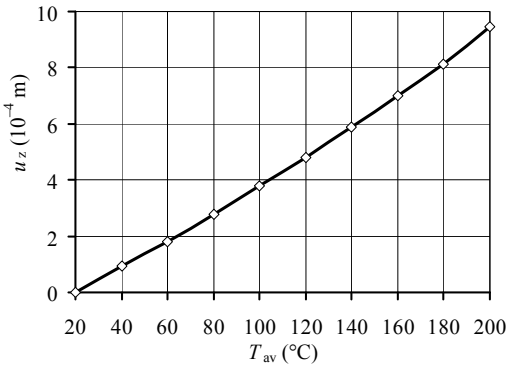

Fig. 14. Dependence of the total thermoelastic shift u_z of the leftmost end of the zinc part on its average temperature T_{av} for $\varsigma = 25$ mm

A similar graph is shown in Fig. 15, depicting the dependence of the average temperature rise ΔT of the zinc part on the shift u_z of its leftmost end (the previous electromagnetic shift ς being 25 mm again). This dependence may be very useful for an accurate determination of this shift (because the average temperature rise of the zinc part may be well measured either indirectly or by thermocouples).

Of great importance are also the dynamic characteristics of the system, because the thermoelastic regime can take tens of seconds or even minutes. Figure 16 shows the time

evolution of the average temperature T_{av} of the zinc part of the plunger for three different field current densities $J_{\mathrm{ext,AC}}$ of frequency $f = 5$ kHz, shift ς being 25 mm. Figure 17 shows the corresponding time evolutions of the shift u_z of the leftmost end of the zinc part of the plunger, the other parameters remaining the same.

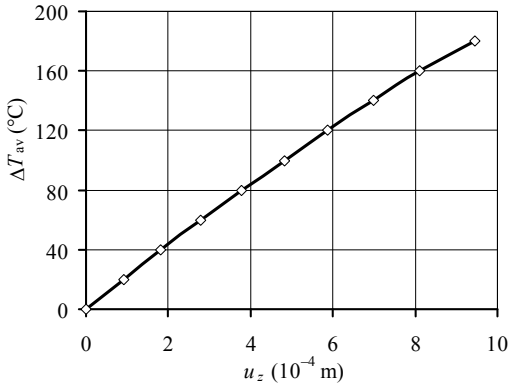

Fig. 15. Dependence of the average temperature rise ΔT_{av} of the zinc part on shift u_z of the leftmost end of this zinc part for $\varsigma = 25$ mm

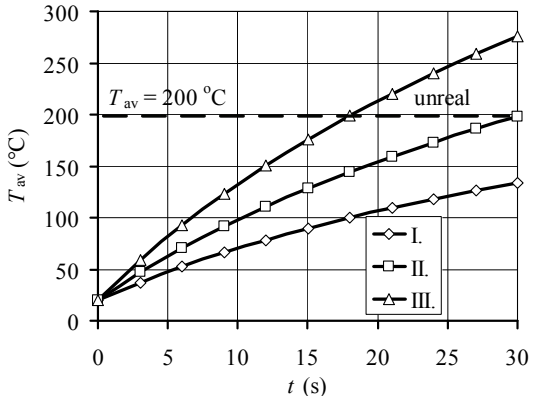

Fig. 16. Time evolution of the average temperature T_{av} of the zinc part of the plunger for three different field current densities ($\varsigma = 25$ mm, $f = 5$ kHz): I - $J_{\mathrm{ext,AC}} = 4\times10^6$ A/m^2, II - $J_{\mathrm{ext,AC}} = 5\times10^6$ A/m^2, III - $J_{\mathrm{ext,AC}} = 6\times10^6$ A/m

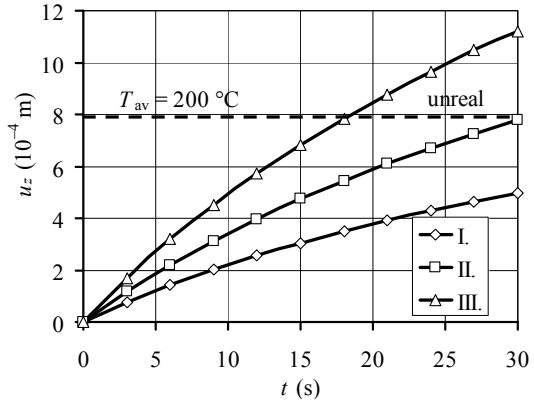

Fig. 17. Time evolution of the shift u_z of the leftmost part of the zinc part of the plunger for three different field current densities ($\varsigma = 25$ mm, $f = 5$ kHz): I - $J_{\mathrm{ext,AC}} = 4\times10^6$ A/m^2, II - $J_{\mathrm{ext,AC}} = 5\times10^6$ A/m^2, III - $J_{\mathrm{ext,AC}} = 6\times10^6$ A/m

The temperature in the system must not exceed 200 °C because of the thermal endurance of used insulation elements. This is also marked in both Figs. 16 and 17 by the unreal zones.

But even these results are far from being complete, because the above figures show the graphs just for several selected parameters. Some more results obtained for other parameters are listed in Table 2.

Table 2. Results for various other parameters (symbol p denoting the volumetric losses in the zinc part of the plunger)

f (Hz)	p (W/m^3)	T_{av} (°C)	$u_{z,\max}$ (m)
$J_{\mathrm{ext,AC}} = 2\times10^6$ A/m^2			
50	1.09×10^3	29.6	4.20×10^{-5}
500	1.06×10^5	32.6	5.40×10^{-5}
5000	4.98×10^6	116. 0	4.14×10^{-4}
$J_{\mathrm{ext,AC}} = 5\times10^6$ A/m^2			
50	6.80×10^3	76.9	2.47×10^{-4}
500	6.64×10^5	98.3	3.40×10^{-4}
5000	3.11×10^7	**870.0**	2.59×10^{-3}

The last row in the table is unreal because of unacceptably high temperature.

Conclusion

The device exhibits a lot of possibilities of practical applications in optics (setting of focal distances of lens systems), laser technologies (setting of position of the laser head or focusing of the laser beam) or microscope technologies (setting of positions of specimens with respect to the focus of light or electron beams). Next work in the domain will be aimed at further acceleration of computations and detailed analysis of behavior of other parts of the device (both clutches).

Acknowledgment

The financial support of the Grant Agency of the Czech Republic (project No.102/09/1305) and Research Plan MSM 6840770017 is gratefully acknowledged.

REFERENCES

[1] Dolezel, I., Karban, P., Ulrych, B, Pantelyat, M., Matyukhin, Y., Gontarowskiy, P. (2007) "Computer model of thermoelastic actuator solved as coupled contact problem", *COMPEL,* Vol. 26 No. 4, pp. 1063–1072.

[2] Dolezel, I., Karban, P., Ulrych, B, Pantelyat, M., Matyukhin, Y., Gontarowskiy, P., Shulzhenko, N. (2008) "Limit operation regimes of actuators working on principle of thermoelasticity", *IEEE Trans. Magn.* Vol. 44 No. 6, pp. 810–813.

[3] Stratton, J. A. (2007), *Electromagnetic Theory*, John Wiley & Sons, Inc., Hoboken, NJ.

[4] Holman, J. P. (2001), *Heat Transfer*, McGrawHill, New York, NY.

[5] Boley, B., Wiener, J. (1960) *Theory of Thermal Stresses*, Wiley, New York, NY.

[6] www.quickfield.com.

[7] www.mathworks.com.

***Authors**: Prof. Ivo Doležel, Academy of Sciences of the Czech Republic, Institute of Thermomechanics, v.v.i., Dolejškova 5, 182 00 Praha 8, Czech Republic, E-mail: dolezel@fel.cvut.cz; Assoc. Prof. Bohuš Ulrych, Dr. Václav Kotlan, University of West Bohemia, Faculty of Electrical Engineering, Univerzitní 26, 306 14 Plzeň, Czech Republic, E-mail: {ulrych, vkotlan}@kte.zcu.cz.*